



OPEN

Tuning the metal-insulator crossover and magnetism in SrRuO₃ by ionic gating

Hee Taek Yi¹, Bin Gao¹, Wei Xie², Sang-Wook Cheong^{1,3} & Vitaly Podzorov^{1,4}

SUBJECT AREAS:

ELECTRONIC PROPERTIES
AND MATERIALSELECTRONIC AND SPINTRONIC
DEVICESMAGNETIC PROPERTIES AND
MATERIALS

MAGNETIC MATERIALS

¹Department of Physics and Astronomy, Rutgers University, Piscataway, New Jersey 08854, USA, ²Department of Chemical Engineering and Materials Science, University of Minnesota, Minneapolis, Minnesota 55455, USA, ³Rutgers Center for Emergent Materials (RCEM), Rutgers University, Piscataway, New Jersey 08854, USA, ⁴Institute for Advanced Materials and Devices for Nanotechnology (IAMDN), Rutgers University, Piscataway, New Jersey 08854, USA.

Received
24 July 2014Accepted
22 September 2014Published
13 October 2014

Correspondence and
requests for materials
should be addressed to
V.P. (podzorov@
physics.rutgers.edu)

Reversible control of charge transport and magnetic properties without degradation is a key for device applications of transition metal oxides. Chemical doping during the growth of transition metal oxides can result in large changes in physical properties, but in most of the cases irreversibility is an inevitable constraint. Here we report a reversible control of charge transport, metal-insulator crossover and magnetism in field-effect devices based on ionically gated archetypal oxide system - SrRuO₃. In these thin-film devices, the metal-insulator crossover temperature and the onset of magnetoresistance can be continuously and reversibly tuned in the range 90–250 K and 70–100 K, respectively, by application of a small gate voltage. We infer that a reversible diffusion of oxygen ions in the oxide lattice dominates the response of these materials to the gate electric field. These findings provide critical insights into both the understanding of ionically gated oxides and the development of novel applications.

Strongly correlated transition metal oxides are known for their rich physics, including ferromagnetism (FM), metal-insulator transition (MIT), high-temperature superconductivity, colossal magnetoresistance and multiferroicity^{1–3}. Achieving control over these phenomena is one of the most pursued goals in condensed matter physics and materials science^{4,5}. Recently, ionic liquid (IL) gating of organic semiconductors and inorganic oxides has been used to induce high densities of charge carriers (over 10¹⁴ cm⁻²) in these materials by an external electric field^{4,6–11}. However, the mechanism of IL gating in transition metal oxides is still unclear, with the electrostatic and electrochemical doping mechanisms debated^{7–13}. For instance, there are conflicting interpretations of IL gating effect on the metal-insulator transition in VO₂. Nakano *et al.* interpreted gating induced modulations of metal-insulator transition as originated from the electrostatically induced surface charge accumulation that mediates bulk structural phase transformation over a macroscopic length scale¹⁰. On the contrary, Jeong *et al.* argued that IL gating leads to electrochemical doping, in which oxygen vacancies are created or annihilated in VO₂¹¹. Indeed, when a gate voltage of a few volts is applied to the ionic liquid, electric field generated at the IL-VO₂ interface can be sufficiently high to force oxygen ions to drift in or out of the oxide. Depending on the physical properties of a particular oxide and the experimental conditions, either of these mechanisms could be relevant, or a combination of two may govern the field-induced phenomena in ionically gated oxides.

SrRuO₃ (SRO) is the most popular strongly correlated conducting oxide, with a FM transition temperature (T_{FM}) of ~160 K, that can be seamlessly integrated with other oxides in oxide heterostructure electronics^{14,15}. In addition, SRO is well known among oxides for the very high stability of its oxidative state (see [14–16] and refs. therein). Modifications of magnetic and transport properties of (ungated) SRO thin films were demonstrated by varying film thickness, partial pressure of O₂ during the film growth and chemical doping^{15–18}. For instance, lower T_{FM} were observed in SRO films grown under low oxygen partial pressure, which can be explained by the presence of oxygen vacancies¹⁶. When oxygen vacancies are created, the average SRO unit cell volume increases, because the structure is relaxed by losing the bonding. Consequently, the orbital overlap between the ruthenium *d*-orbitals and oxygen *p*-orbitals is reduced, leading to a smaller density of states at the Fermi level and a lower ferromagnetic transition temperature relatively to T_{FM} of the stoichiometric SRO. Metal-insulator crossover in (ungated) SRO has also been reported, with a metallic state ($dp/dT > 0$) gradually transforming into an insulating one ($dp/dT < 0$). The metal-insulator crossover temperature, T_{MI} , increases, when the film thickness is reduced or the level of chemical impurities increases^{15,18}. It is believed that T_{MI} in this system is strongly affected by disorder. For instance, in SrTi_{*x*}Ru_{1-*x*}O₃, increasing *x* induces a weak localization that eventually drives the system into an



insulating state with a Mott-type variable range hopping transport - a behavior governed by a combination of disorder and electron correlations¹⁸.

Here we investigate the effect of electric field gating on charge transport and magnetic properties of SRO films by using ionically gated devices that utilize the recently developed facile “cut and stick” semi-solid ion gels (IG)¹⁹. This new method has substantially improved the mechanical integrity of ionically gated devices and allowed us for the first time to observe modulations of the metal-insulator crossover and ferromagnetism in SRO with a gate voltage.

Results

Ionically gated 10-monolayer (4 nm-thick) SRO films. The configuration of our ionically gated SRO devices is shown in Fig. 1 (for fabrication details see Methods). In brief, a few monolayer (ML)-thick SRO thin films were grown on single-crystal SrTiO₃ substrates by a pulsed laser deposition (PLD). Atomic force microscopy (AFM) reveals that the surface of these few nm-thick SRO films is smooth, with atomic terraces of the underlying strontium titanate substrate clearly visible. Source and drain contacts were deposited on SRO by sputtering Au through a shadow mask, and a 10 μm-thick film of ion gel was attached on top of the sample, covering the area between the contacts (the channel). Flexible Au gate was then attached on top of the ion gel. Figure 1 also shows SRO crystal structure and the chemical structure of the ion gel. The cations and anions of the gel ([EMI]⁺ and [TFSA]⁻, respectively) are caged in a neutral polymer matrix, resulting in a semi-solid, easy-to-handle gel that makes device fabrication convenient and provides an effective capacitance of 4 μF·cm⁻², comparable to that of the best ILs¹⁹.

To investigate the electric field effect in SRO, we have first measured the source-drain current, I_{SD} , while sweeping the gate voltage, V_G , in close loops between -2 and 2 V starting at $V_G = 0$ and at a V_G -sweep rate of 0.25 mV·s⁻¹ (5 mV steps in 20 s intervals). Room temperature $I_{SD}(V_G)$ characteristics exhibit a pronounced hysteresis, as shown in Fig. 2a. The sample's initial sheet resistivity per square, ρ , (that is, ρ before gating) is 800 Ω. With increasing gate voltage, I_{SD} increases superlinearly with a threshold-like onset (sec. 1 of

Supplementary Information)¹², resulting in a more conducting state that persists even when V_G is reduced back to 0. A further decrease of V_G to -2 V results in the original more resistive state of the sample with $\rho \approx 800$ Ω. Additional tests reveal that resistivity modulations with V_G are persistent, as long as the devices are kept in high vacuum, but quickly decay if the ion gel is removed and SRO is exposed to air (sec. 2 and 3 of Supplementary Information). This behavior is consistent with redox reactions at the ion-gel/SRO interface.

The ionic gate “leakage” current (that is, an electrolytic displacement current), I_G , recorded during these measurements was about 10⁻⁸ A, which is negligible compared to the induced modulations in I_{SD} in the entire V_G sweep range ($\delta I_{SD}/I_G > 10^3$). This clearly shows that the source-drain conductance modulation in our devices is not an artifact of the gate leakage. It is worth noting that water related impurities in ionic liquids may lead to artifacts in measurements of IL/oxide devices, as pointed out recently^{20,21}. To prevent such effects, all the measurements in this work have been carried out in a “dry” state of ion-gel/SRO devices in high vacuum (sec. 4 of Supplementary Information, Methods). In addition, control experiments with ion-gel gated devices based on other (non-oxide) materials (single crystals of rubrene and WSe₂) have been carried out (sec. 5 and 9 of Supplementary Information). These control tests indicate that the effects observed in our ion-gel/SRO are not related to water contamination. The main contribution to the displacement current, I_G , comes from the motion of the molecular ions ([EMI]⁺ and [TFSA]⁻) of the ion gel in response to an applied V_G (the so-called polarization of ionic liquids)¹⁹. This response is very fast: the capacitance (~4 μF·cm⁻²) of the ion gel remains almost frequency independent up to 100 kHz¹⁹. The reason the displacement process contributing to I_G in the lower panel of Fig. 2a does not seem to saturate is that V_G in this measurement is constantly changing (in a slow sweep), thus causing the ion gel polarization to follow V_G with a similar rate.

Figure 2b shows the temperature dependence of resistivity measured at several fixed values of $V_G = 0, 2.2$ and -2.2 V, that is, at the states marked by the three colored symbols on the room-temperature hysteresis loop (Fig. 2a). V_G was always applied at room temperature before measuring $\rho(T)$. The normalized sheet resistivity, ρ/ρ_{260K} , plotted as a function of T clearly shows a shift of T_{MI} with V_G . T_{MI} is defined as the temperature, at which resistivity reaches the minimum, $d\rho/dT = 0$ (see also Supplementary Fig. S6). At $V_G > 0$, SRO film becomes more conducting with a lower T_{MI} (red curve), compared to the state at zero gate voltage. At $V_G = -2.2$ V, $\rho(T)$ dependence of the sample resembles that at $V_G = 0$ (green and black curves), consistent with the hysteresis in $I_{SD}(V_G)$ measurements in Fig. 2a. The inset in Fig. 2b shows T_{MI} as a function of V_G obtained from a series of $\rho(T)$ measurements at different V_G values. It is clear that the metal-insulator crossover temperature can be tuned in a wide range of $50 < T_{MI} < 120$ K by application of a small gate voltage, $-2.2 < V_G < 2.2$ V. In addition, modulations of ρ with V_G are quantitatively and qualitatively different on the insulating and metallic sides of the crossover (sec. 6 of Supplementary Information). We have systematically observed the effect of gating on the metal-insulator crossover in our 6 ML and 10 ML SRO samples. It's worth noting that we have not detected any kink in $\rho(T)$ in our as-grown SRO samples before applying ion gel (sec. 7 of Supplementary Information). A kink in $\rho(T)$ is believed to be associated with a ferromagnetic transition in the magnetic structure of SRO^{15,17}. Nevertheless, our magnetization measurements, $M(T)$, clearly show a ferromagnetic transition in our SRO films with the FM onset temperature, $T_{FM} \sim 100$ K (sec. 8 of Supplementary Information). We believe the insulating state observed in $\rho(T)$ below T_{MI} and the absence of the kink in the resistivity measurements in our samples are related to disorder.

Figure 2c shows the magnetoresistance (MR) that we define as $\Delta\rho/\rho \equiv (\rho_{B \neq 0} - \rho_{B=0})/\rho_{B=0}$. It is measured in a 10 ML SRO film

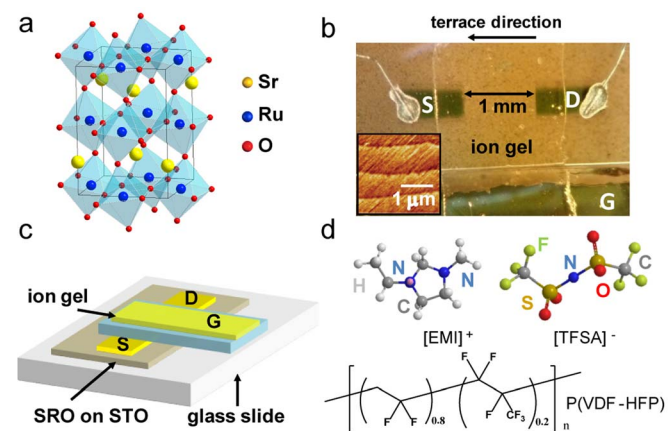


Figure 1 | Ion-gel gated SrRuO₃ (SRO) thin film transistors. (a) SrRuO₃ has an orthorhombic structure with Ru inside the octahedral cage of six oxygen atoms. (b) Optical microphotograph of an ion-gel gated SRO device (before gate lamination) with an inset showing AFM image of a 4 nm-thick (10-monolayer) SRO grown at TiO₂-terminated single-crystal SrTiO₃ substrate. The topography clearly shows a smooth film that continuously coats the substrate terraces without a detrimental 3D growth. (c) Schematics of the ion-gel gated SRO transistor. S, D and G denote the source, drain and gate electrodes, respectively. The gate is formed by laminating a metalized 2.5 μm-thick Mylar film on top of the ion gel. (d) Chemical structure of the ion gel components used in this study.

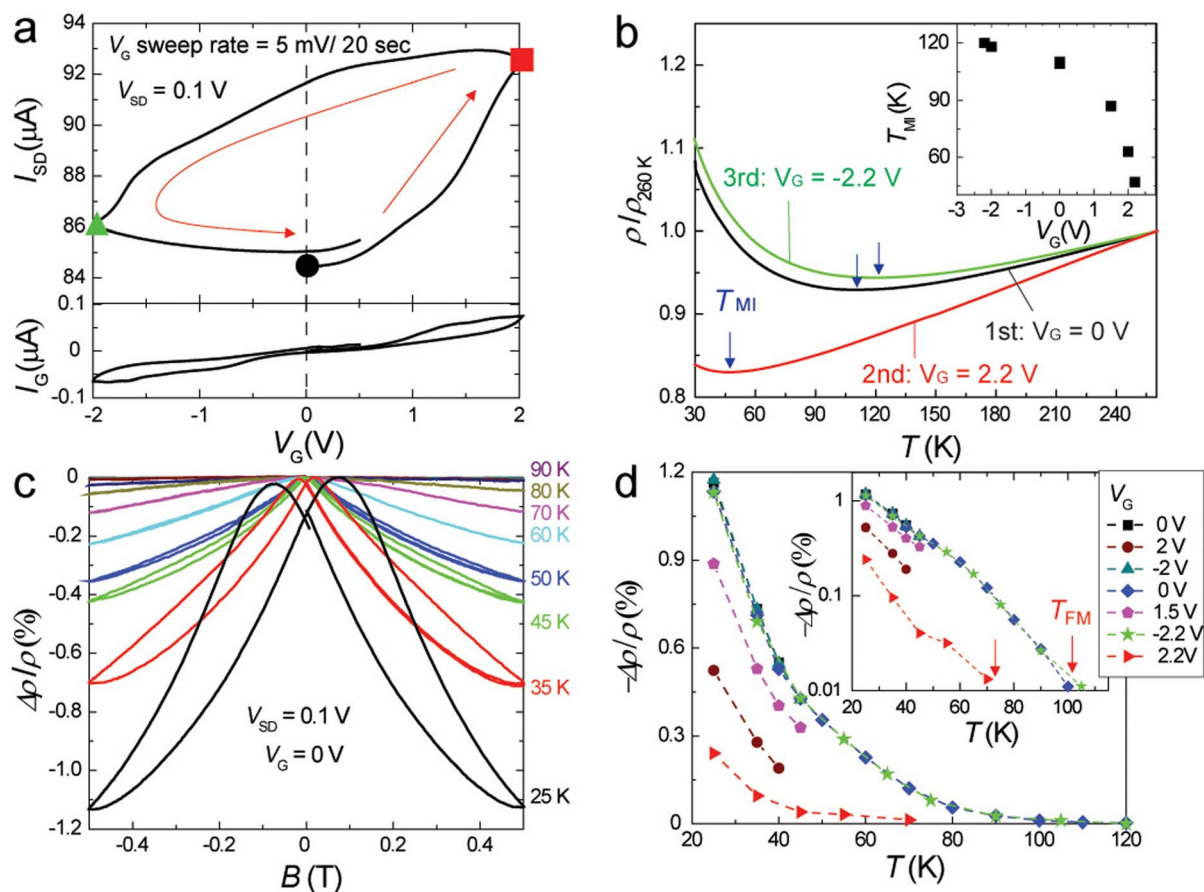


Figure 2 | Charge transport and magnetic properties of ionically gated 10-monolayer SrRuO₃. (a) Gate voltage dependence of the source–drain current (top) and gate leakage current (bottom) at room temperature (V_G sweep rate is 0.25 mV·s⁻¹). (b) Resistivity as a function of temperature measured at $V_G = 0, 2.2,$ and -2.2 V. T_{MI} (arrows) shifts to lower temperatures with positive V_G applied to the ion gel. The inset shows T_{MI} as a function of V_G obtained in the following gating sequence: $V_G = 0, 2, -2, 0, 1.5, -2.2$ and 2.2 V. (c) Magnetic field dependence of magnetoresistance ($\Delta\rho/\rho$) at various temperatures and $V_G = 0, V_{SD} = 0.1$ V. Magnetic field of up to ± 0.5 T was applied perpendicular to the film surface. (d) Temperature dependence of magnetoresistance, $\Delta\rho/\rho(T)$, obtained in 0.5 T at various V_G . The systematic shift of the magnetoresistance onset toward lower temperatures is observed for $V_G > 0$, while the changes at $V_G < 0$ are negligible. The inset shows a semi-log plot of the same data. The magnetoresistance onset temperature, T_C , is defined as the temperature, at which $-\Delta\rho/\rho$ drops below 0.01% (red arrows).

at various temperatures and fixed $V_G = 0$ (ungated device) and $V_{SD} = 0.1$ V. The MR is negative, and at 25 K it clearly shows a hysteresis with minima at the field of magnetic coercivity, $H_C \sim 1$ kOe (black curve). On warming, the hysteresis and MR both reduce. Figure 2d shows the MR measured at $B = 0.5$ T as a function of temperature at the following sequence of gate voltages: $V_G = 0, 2, -2, 0, 1.5, -2.2$ and 2.2 V. With positive gate voltage, the MR curves systematically shift toward lower temperatures (magenta, brown and red symbols). However, when a negative V_G is applied (green stars), the system returns to the initial state corresponding to $V_G = 0$ (blue diamonds and black squares). Note that since the field effect in this system depends on V_G and the gating history, the absolute value of the compensating gate voltage or stressing time have to be adjusted in order to bring the system back to the initial state. The inset is a semi-log plot of the same MR(T) data. Here, we can define the so-called onset of magnetoresistance, characterized by the temperature, T_C , at which $\Delta\rho/\rho$ drops below 0.01%, as indicated in the inset by the red arrows. Below this value, MR is very difficult to determine accurately. T_C defined in such a way is consistent with the ferromagnetic transition temperature, T_{FM} , obtained from the magnetization measurements (sec. 8 of Supplementary Information). Note that it has been reported that T_{FM} in (ungated) SRO can be modified by chemical doping at Ru site with various transition metals, and the onset temperature of MR consistently followed the change in T_{FM} ¹⁷. This

suggests that electrical measurements (that is, magnetoresistance and its onset at T_C) can be used to (indirectly) identify the ferromagnetic phase transition and its temperature T_{FM} . The onset of magnetoresistance in our SRO devices can be systematically shifted between about 70 and 100 K by applying a small gate voltage of $|V_G| \leq 2.2$ V to the ion gel.

Ionically gated 6-monolayer SRO films. It has been previously observed that resistivity and the metal–insulator crossover in (ungated) SRO thin films strongly depend on the film thickness: with a decreasing number of layers, ρ and T_{MI} both increase¹⁵. Furthermore, it has been shown that when the film thickness is reduced to 4–5 MLs, the sample’s resistivity can increase by more than 8 orders of magnitude, compared to thicker samples, and it becomes insulating in the entire accessible temperature range, $T < 300$ K¹⁵. In order to verify that similar thickness-dependent effects take place in our gated SRO devices, we have performed transport measurements in a device based on a thinner (6 ML) film (Fig. 3). $\rho(T, V_G)$ of the 6 ML SRO device shows that the film is about 3 times more resistive than the 10 ML device (zero- V_G sheet resistivity is 2.4 k Ω at 270 K), and its T_{MI} (~ 210 K) is twice as high as that of the 10 ML sample. The shift of T_{MI} to a higher temperature is related to a greater disorder typical for thinner films. Indeed, in very thin films, disorder related to defects, twin domains and FM domain

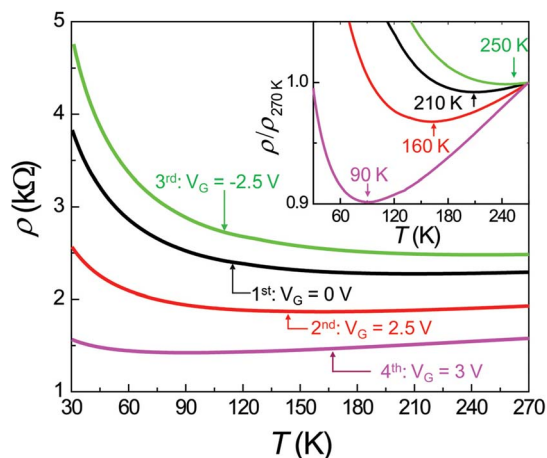


Figure 3 | Temperature dependence of resistivity of 6-monolayer SrRuO₃ at different gate voltages. $\rho(T)$ was measured in the following order: $V_G = 0$ (black), 2.5 (red), -2.5 (green), and 3 V (magenta). The inset shows the normalized resistivity vs. temperature (the arrows indicate the metal-insulator crossover temperature at different V_G). T_{MI} is reversibly modulated in the range 90–250 K by applying a small gate voltage, $|V_G| \leq 3$ V.

boundaries is more critical, leading to a stronger charge carrier localization. $\rho(T)$ of the 6 ML device was measured at different gate voltages following the sequence: $V_G = 0$ (black), 2.5 (red), -2.5 (green) and 3 V (magenta). The slope of $\rho(T)$ indicates that the behavior of the device at $V_G = 3$ V is metallic in a wide temperature range $T > 90$ K (magenta). However, at $V_G = -2.5$ V, the behavior is insulating in the entire temperature range (green). At the lowest temperature in our measurements (here, 30 K), the sample's resistivity is modulated with V_G by more than a factor of 3. The inset shows the normalized resistivity vs. T : the arrows indicate T_{MI} at various gate voltages. It is obvious that T_{MI} is strongly affected by gating - it changes by more than 150 K with V_G varied from -2.5 to 3 V. The drastic changes in $\rho(T)$ dependence, including the absolute value of ρ and the metal-insulator crossover temperature shown in Fig. 3, clearly indicate that the ion-gel gating allows us to control the metal-insulator crossover in SRO. Note that

the modulation of these properties with V_G is noticeably stronger in the thinner (more insulating) sample.

V_G sweep rate dependence of the field effect in ionically gated SRO devices. In this work, we have demonstrated a control of the resistivity, the metal-insulator crossover and the onset of magnetoresistance in thin films of a strongly correlated oxide, SrRuO₃, achieved in ionically gated field-effect devices. Magnetism in SRO has been interpreted as a Stoner-type itinerant ferromagnetism with the ferromagnetic transition temperature strongly affected by the density of states at the Fermi level and electron-electron interactions¹⁴. Thus, magnetism in SRO can be influenced by adding or removing charge carriers via an electric field effect. In addition, removing oxygen from SRO (that is, generating oxygen vacancies) can reduce the hybridization strength between d -orbitals of ruthenium and p -orbitals of oxygen, leading to a reduced density of states at the Fermi level. Therefore, modulations of T_C and T_{MI} observed in this study can, in principle, be explained by either an electrostatic carrier accumulation or an electrochemical doping (generation of oxygen vacancies). Indeed, when a positive gate voltage is applied to the ion gel, electrons should be electrostatically accumulated in the interfacial layer(s) of SRO, leading to an enhancement of conductivity. Removal of oxygen from transition metal oxides is typically equivalent to an electron doping, and an enhancement of conductivity can also be expected in oxygen deficient samples. Note that an increased conductivity was observed in (ungated) oxygen deficient SRO¹⁶. Other physical properties of transition metal oxides can also drastically change with oxidative state of the system²².

In order to understand which of the above two mechanisms plays the dominant role in the reversible tuning of the metal-insulator crossover and magnetoresistance in our ionically gated SRO, we have examined the V_G -sweep rate dependence of the field effect in our devices (Fig. 4a). Note that the systems dominated by fast electronic carrier accumulation, for instance ZnO FETs, show largely V_G -sweep-rate independent characteristics²³. Such dependence has been found to play a major role in organic field-effect transistors (OFET) based on certain disordered organic semiconductors²⁴. In OFETs, it has been found that the nominal mobility calculated from the slope of transfer characteristics can vary by more than an order of magnitude, depending on how fast V_G is swept²⁴. This effect was ascribed to a gradual relaxation of the injected charge carriers in energetically wide distribution of trap states in disordered organic films, and it

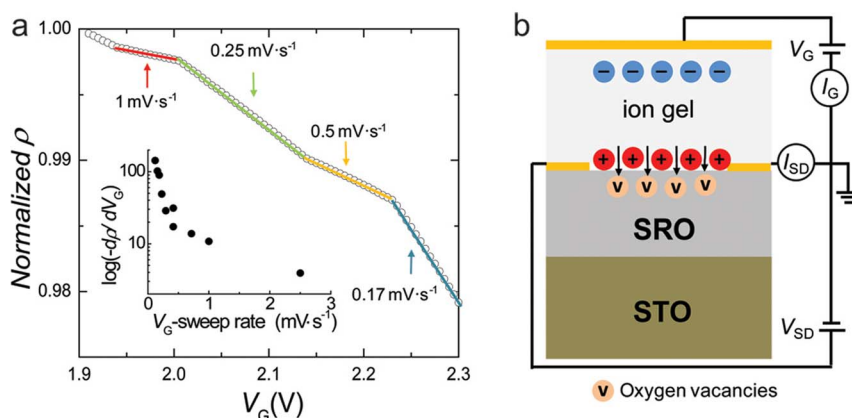


Figure 4 | $\rho(V_G)$ measurements in an ion-gel gated SRO transistor at different V_G sweep rates. (a) $\rho(V_G)$ recorded at room temperature as V_G is increased at different rates, 0.17, 0.25, 0.5 and 1 $\text{mV}\cdot\text{s}^{-1}$ (indicated), corresponding to the time constants of 30, 20, 10 and 5 s between the 5 mV increments in V_G , respectively. The inset shows the resultant dependence of the slope, $d\rho/dV_G$, on the gate voltage sweep rate. (b) Illustration of the mechanism of the electric field effect in ionically gated oxides. When $V_G > 0$ is applied and the ion gel is polarized, negative [TFSA]⁻ ions accumulate near the gate electrode, while positive [EMI]⁺ ions accumulate near the SrRuO₃/ion-gel interface. A strong electric field generated in the top layers of the oxide drives oxygen ions out of the oxide lattice, which is equivalent of generating oxygen vacancies (shown as “v”). These vacancies are responsible for the observed changes in the transport and magnetic properties of ionically gated SRO.



highlights the necessity of more careful data interpretation in OFETs. In our ionically gated SRO, V_G has been swept extremely slowly: in 5 mV increments with a time constant $\tau = 5\text{--}30$ s per increment. Figure 4a shows a normalized resistivity, $\rho(V_G)/\rho(V_G = 1.9\text{V})$, monitored as V_G is swept at different sweep rates, $dV_G/dt = 0.17, 0.25, 0.5$ and $1\text{ mV}\cdot\text{s}^{-1}$ (not in this order), achieved by varying τ while keeping the voltage increment fixed at 5 mV. The inset shows the resultant dependence of the slope of resistivity, $d\rho/dV_G$, on the V_G -sweep rate. The choice of the sweep rates is based on typical diffusion time (10–100 min) of oxygen through a layer with thickness equal to the screening length in SRO (~ 5 Å). It is clear that when the sample is given more time to respond to the changing gate voltage, a greater change in ρ occurs. The most striking observation, however, is an extremely slow dynamics of the sample's response: indeed, the time constants in $\rho(V_G)$ measurement in the main panel of Fig. 4a are $\tau = 5, 10, 20$ and 30 s (per 5 mV increment in V_G). Even at the lowest V_G -sweep rate of $0.17\text{ mV}\cdot\text{s}^{-1}$, corresponding to the longest time constant of 30 s, the effect is far from being saturated: $|d\rho/dV_G|$ is the highest. This dynamics is much slower than that observed in OFETs^{24,25}. Such a remarkably slow process in an inorganic material cannot be rationalized in terms of electronic carrier relaxation in trap states in the FET's accumulation channel. Indeed, charge carrier mobilities in inorganic materials are typically much greater than those in van der Waals organic semiconductors, and thus electronic carrier relaxation is expected to occur much faster here than in OFETs. Ionic motion in the ion gel can not account for such a slow dynamics either: measurements of the capacitance of the ion gel used in this work have shown that its capacitance ($\sim 4\text{ }\mu\text{F}\cdot\text{cm}^{-2}$) remains almost frequency independent up to 100 kHz¹⁹.

V_G sweep rate dependence in layered inorganic (non-oxide) semiconductor, WSe_2 . To exclude any remaining possibility that some extremely slow ionic motion in the ion gel might have caused the observed dynamics in our SRO devices, we have performed a control experiment, in which we used a different (non-oxide) material: layered transition metal dichalcogenide, WSe_2 . Conventional (non-IL) high-mobility field effect transistors based on these layered inorganic semiconductors were demonstrated as early as 2004²⁶. The ionically gated devices were prepared on WSe_2 following the same protocol and using the same ion gel as on SRO, and the field effect, $\rho(V_G)$, was measured at different V_G -sweep rates at otherwise similar conditions (sec. 9 of Supplementary Information). Remarkably, almost no V_G -sweep rate dependence could be detected in these devices (Fig. S9). This confirms that the slow dynamics observed in the SRO transistors is indeed related to the oxygen motion in the oxide. It's important that the strong V_G -sweep rate dependence in SRO FETs is observed both at positive and negative V_G (sec. 9 of Supplementary Information). This indicates that accumulation of either $[\text{TFSA}]^-$ anions or $[\text{EMI}]^+$ cations results in a slow, rate dependent, reversible oxygen drift in the oxide.

Discussion

Several further control experiments lend an additional support to the model of electrochemical oxygen vacancy creation/annihilation. We have measured $\rho(T)$ with V_G applied at 220 K and compared it with the case of V_G applied at room temperature (sec. 10 of Supplementary Information): this experiment clearly shows that there is almost no gating effect and no T_{MI} shift, when V_G is applied at low temperature. In a separate experiment, it was shown that the strength and hysteresis of the field effect in $I_{\text{SD}}(V_G)$ characteristics measured at low temperatures are drastically reduced (sec. 11 of Supplementary Information). In addition, performing measurements of ion-gel/SRO devices in oxygen atmosphere results in a much stronger suppression of conductivity (depletion) at a negative V_G (sec. 12 of Supplementary Information), consistent with the observation in other oxides^{11,27}. Finally, we have estimated the carrier

density expected in purely electrostatic charge accumulation model (following the procedure described in [20]) and that in the electrochemical doping scenario (sec. 13 of Supplementary Information). These calculations show that the electrochemical model describes the operation of ion-gel/SRO devices much better. It is worth noting that although a combination of electrostatic and electrochemical processes has been suspected to govern the field effect in certain IL-gated oxides, disentangling the relative contributions of these effects simply based on $I_{\text{SD}}(V_G)$ loops measured at room temperature has been difficult^{20,21,28}.

The combination of experiments performed in this work leads to a set of observations that are consistent with each other and strongly suggest that the dominant mechanism of the field effect in ionically gated SRO devices is an electric field induced migration of ionic oxygen in SRO lattice (creation and annihilation of oxygen vacancies). A positive gate voltage applied to the ion gel attracts the organic anions to the gate electrode, while the organic cations are accumulated near the interface with SRO (Fig. 4b). The electric field created by the accumulated cations drives the oxygen ions from SRO toward the ion gel, thus creating oxygen vacancies in the oxide. This effect is reversible on changing the gate voltage polarity.

To conclude, we have achieved a gate controlled electrochemical modulation of the metal-insulator crossover and the onset of magnetoresistance (associated with a ferromagnetism) in ion-gel gated thin-film SRO. The temperature of the metal-insulator crossover can be continuously and reversibly tuned in the range 90–250 K (in 6-ML SRO) and 50–120 K (in 10-ML SRO) by applying a small gate voltage, $|V_G| \leq 3$ V. The magnetoresistance onset can also be reversibly shifted by as much as 30 K. We have observed that modulations of ρ with V_G depend strongly on the gate voltage sweep rate, with remarkably long time constants of tens of seconds, which can only be consistent with a slow dynamics of ionic species (such as oxygen) in the oxide lattice. We believe that the observed field effect on the electronic properties of SRO is predominantly governed by the creation and annihilation of oxygen vacancies, rather than an electrostatic accumulation of electrons or holes in SRO. Given the outstanding oxygen stability of SRO, demonstration of these effects in this material indicates that oxygen drift in the lattice might be even stronger in other ionically gated oxides. These fascinating switchable effects in magnetism and the metal-insulator crossover in ionically gated SRO help to improve our fundamental understanding of strongly correlated oxides and may point to novel electronic applications based on these materials.

Methods

SRO thin film growth and device fabrication. 6 and 10 ML (a few nm-thick) SRO thin films were grown on TiO_2 -terminated SrTiO_3 substrates using a pulsed laser deposition. For 10 ML SRO films, a pulsed KrF excimer laser with a power of $2\text{ mJ}\cdot\text{cm}^{-2}$, a repetition rate of 1 Hz and a pulse duration of 10 ns has been used to ablate a target (99.9% SrRuO_3 , MTI Corp.) for 100 s in 50 mTorr of oxygen. The x-ray scattering data for 10 and 70 ML SRO films suggest that our as-deposited samples are slightly oxygen deficient (sec. 14 of Supplementary Information). For the 6 ML samples, the same power and frequency were used for 86 sec in 80 mTorr of oxygen. The film thickness was monitored *in-situ* using a reflection high-energy electron diffraction (RHEED). 60 nm-thick Au source and drain contacts were deposited on top of the SRO film using a *dc* magnetron sputtering through a shadow mask. "Cut and stick" rubbery ion gel layer was placed on top of the SRO sample, overlapping with the contacts. For the gate electrode, a 60 nm-thick gold film was sputtered at the surface of a free-standing $2.5\text{ }\mu\text{m}$ -thick flexible Mylar sheet. The metallized Mylar was then laminated on top of the ion gel (Au facing the gel), thus completing the device fabrication (Fig. 1). The chemical structure of the ion gel used in this study is shown in Fig. 1d. It consists of 1-ethyl-3-methylimidazolium, $[\text{EMI}]^+$, and bis(trifluoromethylsulfonyl), $[\text{TFSA}]^-$, cations and anions, respectively, that are caged in a matrix of poly(vinylidene fluoride-co-hexa-fluoropropylene), P(VDF-HFP)¹⁹. Compared to ionic liquids, ion gels are semi-solid and do not flow, which makes device fabrication convenient. It can be used in any configuration, because ions are trapped in the polymer matrix. Furthermore, ion gels can be easily cut in any shape with a razor blade and applied to any surface of interest, providing an effective capacitance of $\sim 4\text{ }\mu\text{F}\cdot\text{cm}^{-2}$, similar to that of the best ILs.



Electrical measurements. In order to minimize incorporation of water, measurements have been carried out in “dry” conditions: (a) all the components of our devices (SRO films and ion gel) were stored in a dry box, (b) they were exposed to air only for a few minutes during lamination of ion gel on SRO, (c) the assembled devices were quickly loaded into a high-vacuum chamber and pumped with a dry pump to 10^{-6} Torr, where they were kept for at least 3 h before measurements.

Electrical measurements were performed using Keithley source-meters K-2400 and electrometer K-6514 controlled by a LabView program. Advanced Research Systems cryostat and GMW 5403 electromagnet were used for temperature variable magneto-transport measurements. In T -variable measurements, V_G was always changed at room temperature, before the temperature cycling. In $\rho(T)$ measurements, temperature was slowly lowered below 300 K at a controlled rate of 4 K/min in the cryostat while recording $\rho(T)$. Measurements were performed in high vacuum (10^{-6} Torr). The dc magnetization was measured using a superconducting quantum interference device magnetometer (Quantum Design magnetic property measurement system).

- Imada, M., Fujimori, A. & Tokura, Y. Metal-insulator transitions. *Rev. Mod. Phys.* **70**, 1039–1263 (1998).
- Jin, S. *et al.* Thousandfold Change in Resistivity in Magnetoresistive La-Ca-Mn-O Films. *Science* **264**, 413–415 (1994).
- Cheong, S. W. & Mostovoy, M. Multiferroics: a magnetic twist for ferroelectricity. *Nat. Mater.* **6**, 13–20 (2007).
- Ueno, K. *et al.* Field-Induced Superconductivity in Electric Double Layer Transistors. *J. Phys. Soc. Jpn.* **83**, 032001 (2014).
- Ahn, C. H. *et al.* Electrostatic modification of novel materials. *Rev. Mod. Phys.* **78**, 1185–1212 (2006).
- Kim, S. H. *et al.* Electrolyte-Gated Transistors for Organic and Printed Electronics. *Adv. Mater.* **25**, 1822–1846 (2013).
- Dhoot, A. S., Israel, C., Moya, X., Mathur, N. D. & Friend, R. H. Large Electric Field Effect in Electrolyte-Gated Manganites. *Phys. Rev. Lett.* **102**, 136402 (2009).
- Bollinger, A. T. *et al.* Superconductor-insulator transition in $\text{La}_{2-x}\text{Sr}_x\text{CuO}_4$ at the pair quantum resistance. *Nature* **472**, 458–460 (2011).
- Shi, J., Ha, S. D., Zhou, Y., Schoofs, F. & Ramanathan, S. A correlated nickelate synaptic transistor. *Nat. Commun.* **4**, 2676 (2013).
- Nakano, M. *et al.* Collective bulk carrier delocalization driven by electrostatic surface charge accumulation. *Nature* **487**, 459–462 (2012).
- Jeong, J. *et al.* Suppression of Metal-Insulator Transition in VO_2 by Electric Field-Induced Oxygen Vacancy Formation. *Science* **339**, 1402–1405 (2013).
- Zhou, Y. & Ramanathan, S. Relaxation dynamics of ionic liquid- VO_2 interfaces and influence in electric double-layer transistors. *J. Appl. Phys.* **111**, 084508 (2012).
- Fujiwara, K., Ichimura, T. & Tanaka, H. Nonvolatile Transport States in Ferrite Thin Films Induced by Field-Effect Involving Redox Processes. *Adv. Mat. Interfaces* (Admi.201300108).
- Allen, P. B. *et al.* Transport properties, thermodynamic properties, and electronic structure of SrRuO_3 . *Phys. Rev. B* **53**, 4393–4398 (1996).
- Xia, J., Siemons, W., Koster, G., Beasley, M. R. & Kapitulnik, A. Critical thickness for itinerant ferromagnetism in ultrathin films of SrRuO_3 . *Phys. Rev. B* **79**, 140407R (2009).
- Lu, W. *et al.* Effect of oxygen vacancies on the electronic structure and transport properties of SrRuO_3 thin films. *J. Appl. Phys.* **113**, 17E125 (2013).
- Pi, L., Maignan, A., Retoux, R. & Raveau, B. Substitution at the Ru site in the itinerant ferromagnet SrRuO_3 . *J. Phys.: Condens. Matter* **14**, 7391–7398 (2002).
- Kim, K. W., Lee, J. S., Noh, T. W., Lee, S. R. & Char, K. Metal-insulator transition in a disordered and correlated $\text{SrTi}_{1-x}\text{Ru}_x\text{O}_3$ system: Changes in transport properties, optical spectra, and electronic structure. *Phys. Rev. B* **71**, 125104 (2005).

- Lee, K. H. *et al.* “Cut and Stick” Rubbery Ion Gels as High Capacitance Gate Dielectrics. *Adv. Mater.* **24**, 4457–4462 (2012).
- Ha, S. D., Vetter, U., Shi, J. & Ramanathan, S. Electrostatic gating of metallic and insulating phases in SmNiO_3 ultrathin films. *Appl. Phys. Lett.* **102**, 183102 (2013).
- Ji, H., Wei, J. & Natelson, D. Modulation of the Electrical Properties of VO_2 Nanobeams Using an Ionic Liquid as a Gating Medium. *Nano Lett.* **12**, 2988–2992 (2012).
- Jeen, H. *et al.* Reversible redox reactions in an epitaxially stabilized SrCoO_x oxygen sponge. *Nature Mater.* **12**, 1057–1063 (2013).
- Maeng, J. *et al.* Effect of gate bias sweep rate on the electronic properties of ZnO nanowire field-effect transistors under different environments. *Appl. Phys. Lett.* **92**, 233120 (2008).
- Chen, Y. *et al.* Dynamic character of charge transport parameters in disordered organic semiconductor field-effect transistors. *Phys. Chem. Chem. Phys.* **14**, 14142–14151 (2012).
- Chen, Y. & Podzorov, V. Bias Stress Effect in “Air-Gap” Organic Field-Effect Transistors. *Adv. Mater.* **24**, 2679–2684 (2012).
- Podzorov, V., Gershenson, M. E., Kloc, Ch., Zeis, R. & Bucher, E. High-mobility field-effect transistors based on transition metal dichalcogenides. *Appl. Phys. Lett.* **84**, 3301 (2004).
- Schladt, T. D. *et al.* Crystal-Facet-Dependent Metallization in Electrolyte-Gated Rutile TiO_2 Single Crystals. *ACS Nano* **7**, 8074 (2013).
- Ichimura, T., Fujiwara, K. & Tanaka, H. Dual field effects in electrolyte-gated spinel ferrite: electrostatic carrier doping and redox reactions. *Sci. Rep.* **4**, 5818 (2014).

Acknowledgments

HTY and the part of work performed at Rutgers University have been financially supported by DOE BES award under Grant No. DE-SC0005464 (ER46763). SWC and BG are funded by the Gordon and Betty Moore Foundation’s EPiQS Initiative through Grant GBMF4413 to the Rutgers Center for Emergent Materials. We are grateful to C. D. Frisbie and L. C. Feldman for helpful discussions.

Author contributions

H.T.Y. and V.P. designed the experiments. H.T.Y. performed device fabrication and measurements. B.G. and S.W.C. grew SrRuO_3 films. W.X. prepared the ion gel. H.T.Y. and V.P. analyzed the data and wrote the paper. All authors discussed the results and contributed to editing the paper.

Additional information

Supplementary information accompanies this paper at <http://www.nature.com/scientificreports>

Competing financial interests: The authors declare no competing financial interests.

How to cite this article: Yi, H.T., Gao, B., Xie, W., Cheong, S.-W. & Podzorov, V. Tuning the metal-insulator crossover and magnetism in SrRuO_3 by ionic gating. *Sci. Rep.* **4**, 6604; DOI:10.1038/srep06604 (2014).



This work is licensed under a Creative Commons Attribution-NonCommercial-NoDerivs 4.0 International License. The images or other third party material in this article are included in the article’s Creative Commons license, unless indicated otherwise in the credit line; if the material is not included under the Creative Commons license, users will need to obtain permission from the license holder in order to reproduce the material. To view a copy of this license, visit <http://creativecommons.org/licenses/by-nc-nd/4.0/>